IEEE Access
Multidisciplinary | Rapid Review | Open Access Journal

SPECIAL SECTION ON SECURITY AND PRIVACY FOR VEHICULAR NETWORKS

Received November 12, 2017, accepted December 12, 2017, date of publication January 1, 2018, date of current version May 2, 2018.

*Digital Object Identifier 10.1109/ACCESS.2017.2786711*

# Fast Location Algorithm Based on an Extended Symmetry Nested Sensor Model in an Intelligent Transportation System

**XIAOLIN LI, SHIE WU, JIQU HAN, AND WENQI WANG**
School of Opto-Electronic Information Science and Technology, Yantai University, Yantai 264000, China
Corresponding author: Xiaolin Li (lixiaolinshiwo@163.com)

**ABSTRACT** Vehicle positioning has played an important role in intelligent transportation systems. Previous research has had difficulties in increasing the sensor aperture and reducing the computational complexity of the vehicle positioning algorithm. This paper proposes a new sensor model to extend the sensor aperture, which is similar to the nested sensor model combined with fourth-order cumulants. The proposed algorithm estimates the number of vehicles, which is much higher than the actual number of sensors. An ideal characteristic equation-based method is used to avoid the use of eigenvalue decomposition and spectrum peak search, thereby greatly reducing the computation complexity. In addition, the weighted coefficient matrix is introduced for optimization. Theoretical analysis and simulation results show that the proposed algorithm has lower computational complexity, avoids 2-D parameter matching, and has a high utilization of arrays while still ensuring accurate parameter estimation.

**INDEX TERMS** Intelligent transportation system, vehicle detection, sensor systems, the sensor aperture extension, characteristic equation-based method (CEM), weighted coefficient matrix.

## I. INTRODUCTION

An intelligent transportation system is a fundamental approach used to solve the problems of transportation in the world. An intelligent transportation system is produced in the background of the full development and progress of modern science and technology. The real-time positioning of the vehicles facilitates unified management, monitoring, scheduling and so on. Vehicle positioning has played an important role in intelligent transportation systems. In the past few years, source location has received significant attention. Most relevant papers have focused on the estimation of far-field sources [1]–[5], as it is assumed that such an approach greatly simplifies the spatial spectrum estimation. In contrast, there are relatively few studies on near-field sources. In real environments, near-field sources location are typically used in vehicle positioning. Therefore, the study of the localization of near-field sources has started to receive more attention and has achieved many good results. Some specific algorithms [6]–[13] have been presented for near-field sources, such as the two-dimensional (2-D) MUSIC method [14], the maximum likelihood method [15], the path following method [16] and the polynomial rooting method [17]. The high-order ESPRIT method was also presented in reference [18].

Currently, the symmetric sensor model is adopted by most of the traditional algorithms [19]–[21] for near-field sources. Traditional algorithms can lead to a loss of sensor apertures because the number of sources that can be resolved by traditional algorithms is less than the number of the sensors. Additionally, most algorithms require eigen value decomposition (EVD) and a spectrum search, thereby increasing the computational complexity.

In this paper, we present a novel sensor model named the extended symmetry nested sensor (ES-nested), which is similar to the combination of the NEST sensor model [22] with a special high-order cumulants vector to greatly expand the sensor aperture. The proposed algorithm can estimate a much larger number of sources than the number of sensors and adopts the characteristic equation-based method (CEM) [23], [24] instead of EVD and spectrum search. The proposed algorithm can reduce the computational complexity and can also guarantee the estimation precision. The theory shows that the proposed algorithm has a large aperture extension ability and a low computational complexity. The novel sensor model is applied to intelligent transportation, meanwhile it is also applied to Smart grid [25], [26].

The main factors that affect the performance of the proposed algorithm are the precision of the high-order

cumulant vector $z$ and the difference between the elements of $z$. The algorithm can be further improved by introduction of a weighted coefficient matrix $\boldsymbol{W}$ for optimization. The theory shows that the improved algorithm can improve the performance of the proposed algorithm without increasing the computational complexity.

The remainder of the paper consists of five sections. Section 2 briefly reviews the novel sensor model and the signal model. Section 3 introduces the proposed algorithm in further detail. Section 4 introduces the weighted coefficient matrix and provides details on how it can improve the proposed algorithm. Section 5 presents sufficient numerical examples to demonstrate the performance of the proposed algorithm. Section 6 concludes the paper.

## II. SPECIAL SENSOR MODEL AND SIGNAL MODEL

The novel sensor structure used is shown in Figure 1. The sensor model, which contains 2(M+N)+1 omni-directional sensors, is composed of three sub-sensors. Sub-sensor 1 contains 2N+1 omni-directional sensors, with a sensor element spacing of d. Sub-sensor 2 and sub-sensor 3 are located at each side of sub-sensor 1. The distance between the central sensor and the side sensors is (3N+1)d. These two sub-sensors contain M omni-directional sensors, with the sensor element spacing of (2N+1)d. Meanwhile in Figure 1. The solid line represents the real distance, the dotted line represents the virtual distance, and the dotted line contains several sensors.

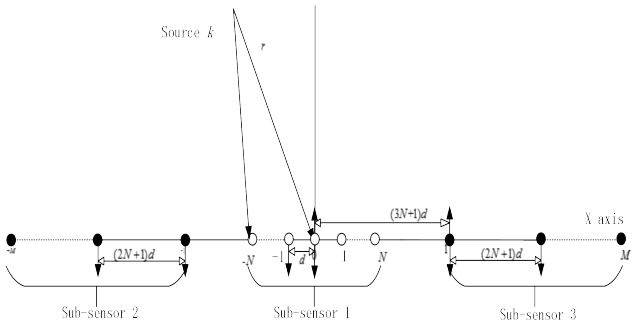


**FIGURE 1.** Special symmetrical linear sensor configuration.

It is assumed that L narrowband sources are impinging on the novel sensor model, as shown in Figure 1. The center of the sensor is considered to be the phase reference point. The data received by sensor $m$ can be expressed as:

$$\boldsymbol{x}_m(t) = \sum_{k=1}^{L} s_k(t) e^{j[o_k p_m + \phi_k p_m^2]} + n_m(t) \quad t = 1, 2, \cdots, K \tag{1}$$

where $K$ is the number of snapshots, $\boldsymbol{s}_k(t)$ is the kth narrowband near-field source, and $\boldsymbol{n}_m(t)$ is the additive Gaussian noise received by the $m$th sensor.

$p_m$ is the distance between the reference sensor and sensor m. $o_k$ and $\phi_k$ can be expressed as follows:

$$o_k = \frac{2\pi d \sin(\theta_k)}{\lambda} \tag{2}$$

$$\phi_k = \frac{\pi d^2 \cos^2(\theta_k)}{\lambda r_k} \tag{3}$$

where $\lambda$ is the wavelength of the near-field sources, and $\theta_k$ and $r_k$ are the DOA and the range of the $k$th near-field sources, respectively.

The vector form of the data received by the sensor can be expressed as:

$$\boldsymbol{X}(t) = \boldsymbol{A}(\theta, r)\boldsymbol{S}(t) + \boldsymbol{N}(t) \tag{4}$$

where $\boldsymbol{X}(t) = [\boldsymbol{x}_1(t), \boldsymbol{x}_2(t), \cdots, \boldsymbol{x}_{2(N+M)+1}(t)]^T$ is the data received by the sensor,

$\boldsymbol{N}(t) = [\boldsymbol{n}_1(t), \boldsymbol{n}_2(t), \cdots, \boldsymbol{n}_{2(N+M)+1}(t)]^T$ is the noise matrix,

$\boldsymbol{S}(t) = [\boldsymbol{s}_1(t), \cdots, \boldsymbol{s}_L(t)]^T$ is the source matrix and $\boldsymbol{A}(\theta, r)$ is the $(2(N+M)+1) \times L$ manifold matrix, which can be expressed as:

$$\boldsymbol{A}(\theta, r) = [\boldsymbol{a}(\theta_1, r_1), \cdots, \boldsymbol{a}(\theta_L, r_L)] \tag{5}$$

where $\boldsymbol{a}(\theta_k, r_k)$ is expressed as:

$$\begin{aligned}\boldsymbol{a}(\theta_k, r_k) = [&\exp(j(p_{-(M+N)}o_k + p^2_{-(M+N)}\phi_k)), \cdots, \\ &\exp(j(p_{(M+N)}o_k + p^2_{(M+N)}\phi_k))]^T \; 1 \le k \le L\end{aligned} \tag{6}$$

In this paper, the following assumptions are made:

(1) The L signals are all statistically independent;
(2) The sensor noise is additive white Gaussian noise, which is independent of the signal sources.
(3) The minimum sensor spacing d is less than a quarter-wavelength.

## III. PROPOSED ALGORITHM

### A. DOA ESTIMATION OF NEAR-FIELD SOURCES

In this section, a special cumulant matrix is constructed to obtain the angle of the near-field source estimation based on the characteristics of high-order cumulants. Based on the assumptions above, we define the fourth-order cumulant as

$$\begin{aligned}\boldsymbol{C}(m, -m, n, -n) &= \mathrm{cum}\{x_m, x^*_{-m}, x^*_n, x_{-n}\} \\ &= \sum_{i=1}^{L} c_{4si} a_i(m) a_i^*(-m) a_i^*(n) a_i(-n) \\ &= \sum_{i=1}^{L} c_{4si} \exp(j(2(p_m - p_n)o_i))\end{aligned} \tag{7}$$

where $c_{4si}$ is expressed as:

$$c_{4si} = \mathrm{cum}(s_i(t), s_i(t), s_i(t), s_i(t))$$

In contrast with the traditional algorithms, the proposed algorithm utilizes the novel sensor model to construct fewer

$$\boldsymbol{C}_1 = \begin{bmatrix} z1(0) & z1(-1) & z1(-2) & \cdots & z1(-2N) \\ z1(1) & z1(0) & z1(-1) & \cdots & z1(-2N+1) \\ z1(2) & z1(1) & z1(0) & \cdots & z1(-2N+2) \\ \vdots & \vdots & \vdots & \ddots & \vdots \\ z1(2N) & z1(2N-1) & z1(2N-2) & \cdots & z1(0) \end{bmatrix} \tag{10}$$

cumulant elements to obtain a higher utilization of sensors and a lower computational complexity.

Sub-sensor 1 is first utilized to construct the cumulant matrix $\boldsymbol{C}_1$ as follows:

$$\begin{aligned} \boldsymbol{C}_1(m,n) &= \text{cum}\{x_m, x_{-m}^*, x_n^*, x_{-n}\} \\ &= \sum_{i=1}^{L} c_{4si}\exp(j2(p_m - p_n)o_i) \\ &= \sum_{i=1}^{L} c_{4si}\exp(j2(m-n)o_i)m, \quad n \in [-N, N] \end{aligned} \tag{8}$$

The following function is then defined to facilitate the derivation of the proposed algorithm:

$$z1(i) = \sum_{i=1}^{L} c_{4si}\exp(j2io_i) \quad i \in [-2N, 2N] \tag{9}$$

From equation (9), it can be seen that the high-order cumulant matrix $\boldsymbol{C}_1$ is a complex Toeplitz matrix. Therefore, the $\boldsymbol{C}_1$ matrix can be expressed in (10), as shown at the top of this page.

An estimate of the vector $z1$ can be obtained by adding the oblique diagonal elements of matrix $\boldsymbol{C}_1$.

When $k = -1, -2, \cdots, -2N$:

$$z1(k) = \frac{1}{(2N+1+k)} \sum_{q=1}^{2N+1+k} \boldsymbol{C}_1(q, q-k) \tag{11}$$

When $k = 0, 1, \cdots, 2N$:

$$z1(k) = \frac{1}{(2N+1-k)} \sum_{q=1}^{2N+1+k} \boldsymbol{C}_1(q, q-k) \tag{12}$$

Sub-sensor 1 and sub-sensor 2 are then used to construct the M(2N+1) dimensional high-order cumulant matrix $\boldsymbol{C}_2$ as follows:

$$\begin{aligned} &\boldsymbol{C}_2(m,n) \\ &= \text{cum}\{x_m, x_{-m}^*, x_n^*, x_{-n}\} \\ &= \sum_{i=1}^{L} c_{4si}\exp(j2(p_m - p_n)o_i) \\ &m \in [-M-N-1, -N-1], \quad n \in [-N, N] \\ &\longrightarrow (p_m - p_n) \in [-(2MN+M+2N), -(2N+1)] \end{aligned} \tag{13}$$

The high-order cumulant matrix $\boldsymbol{C}_2$ is then vectored to obtain the new vector $z2$, which can be expressed as follows:

$$z2 = \text{vec}(\boldsymbol{C}_2) \tag{14}$$

Namely:

$$\begin{aligned} &z2((2N+1)(i-1)+k) = \boldsymbol{C}_2(i,k) \\ &= \sum_{i=1}^{L} c_{4si}\exp(j2(p_{-i-N} - p_{k-N-1})o_i) \\ &= \sum_{i=1}^{L} c_{4si}exp(j2((-i-1)(2N+1) - (3N+1) \\ &\quad -(k-1-N))o_i) \\ &\quad i = 1, \cdots, M; \quad k = 1, 2, \cdots, 2N+1 \end{aligned} \tag{15}$$

Sub-sensor 1 and sub-sensor 3 are then used to construct the M(2N+1) dimensional high-order cumulant matrix $\boldsymbol{C}_3$ as follows:

$$\begin{aligned} \boldsymbol{C}_3(m,n) &= cum\{x_m, x_{-m}^*, x_n^*, x_{-n}\} \\ &= \sum_{i=1}^{L} c_{4si}\exp(j2(p_m - p_n)o_i) \\ m &\in [N+1, M+N+1], \quad n \in [-N, N] \\ &\longrightarrow (p_m - p_n) \in [(2N+1), (2MN+M+2N)] \end{aligned} \tag{16}$$

The high-order cumulant matrix $\boldsymbol{C}_3$ is then vectored to obtain the new vector $z3$, which can be expressed as follows:

$$z3 = \text{vec}(\boldsymbol{C}_3) \tag{17}$$

Namely:

$$\begin{aligned} &z3((2N+1)(i-1)+k) = \boldsymbol{C}_3(i,k) \\ &= \sum_{i=1}^{L} c_{4si}\exp(j2(p_{i+N} - p_{n-N-1})o_i) \\ &= \sum_{i=1}^{L} c_{4si}\exp(j2((i-1)(2N+1) + (3N+1) \\ &\quad -(k-1-N))o_i) \\ &\quad i = 1, \cdots, M; \quad n = 1, 2, \cdots, 2N+1 \end{aligned} \tag{18}$$

The high-order cumulant vectors $z1$, $z2$ and $z3$ are recombined to obtain the $(4N+1)+2(2N+1)M$ dimensional high-order cumulant vector $z$ as follows:

$$z = [z2 \ z1 \ z3] \tag{19}$$

where

$$z(i) = \sum_{i=1}^{L} c_{4si}\exp(j2io_i) \ i \in [-(2N+(2N+1)M), 2N+(2N+1)M]$$

There are three main factors that cause the traditional algorithms to have high computational complexity: construction of the high-order cumulant matrix, the eigenvalue decomposition and the one-dimensional or multidimensional spectrum peak search. The proposed algorithm reduces the computational complexity by using the CEM method for simplification, thus removing the requirement for eigenvalue and spectrum searching. This method will now be discussed in more detail.

First, an L-order polynomial is constructed as follows:

$$f(\chi)=\prod_{k=1}^{L}(\chi-e^{(j2o_k)})=\chi^L+c_{L-1}\chi^{L-1}+\cdots+c_1\chi^1+c_0 \tag{20}$$

It can be easily seen that the L roots of the polynomial in equation (20) correspond to the angle information of the near-field sources. Therefore, the coefficient of this polynomial $[c_{L-1}, c_{L-2}, \cdots, c_0]$ must be obtained to construct the polynomial in equation (20); the angle information can be obtained by solving this equation.

Based on the relationship between the angle information and the polynomial, we can summarize the parameter estimation method in three steps: (1) obtain the high-order cumulant vector $z$; (2) obtain the polynomial coefficient and convert it into the polynomial $f(\chi)$; (3) obtain the roots of the polynomial and transform these roots into the angle information of the near-field sources. The derivation process of the proposed algorithm is given as follows.

For the convenience of the derivation process of the proposed algorithm, set $P=2N+(2N+1)M$.

Because $e^{j2o_k}k=1,2,\cdots,L$ are the solutions to equation (20), the following K equalities hold:

$$e^{j2o_kL}+c_{L-1}e^{j2o_k(L-1)}+\cdots+c_1e^{j2o_k}+c_0=0 \qquad k=1,2,\cdots,L \tag{21}$$

Multiplying both sides of equation (21) with $c_{4si}e^{j2o_kJ}$ for different values of k and J yields:

$$\begin{cases} c_{4s1}e^{j2o_1J}e^{j2o_1L}+c_{4s1}e^{j2o_1J}c_{L-1}e^{j2o_1(L-1)}+\cdots \\ +c_{4s1}e^{j2o_1J}c_1e^{j2o_1}+c_{4si}e^{j2o_1J}c_0=0 \\ \vdots \\ c_{4sL}e^{j2o_LJ}e^{j2o_LL}+c_{4sL}e^{j2o_LJ}c_{L-1}e^{j2o_L(L-1)}+\cdots \\ +c_{4sL}e^{j2o_LJ}c_1e^{j2o_L}+c_{4sL}e^{j2o_LJ}c_0=0 \end{cases} \qquad J=-P,\cdots 0,\cdots,P-L \tag{22}$$

Taking the sum of (22) for each value of $k=1,2,\cdots,L$ yields:

$$\begin{aligned} &\sum_{i=1}^{L}c_{4si}e^{j2o_iJ}e^{j2o_iL}+\sum_{i=1}^{L}c_{4si}e^{j2o_iJ}c_{L-1}e^{j2o_i(L-1)} \\ &\quad+\cdots+\sum_{i=1}^{L}c_{4si}e^{j2o_iJ}c_1e^{j2o_i}+\sum_{i=1}^{L}c_{4si}e^{j2o_iJ}c_0=0 \\ &J=-P,\cdots 0,\cdots,P-L \end{aligned} \tag{23}$$

Substituting (19) into (23) yields a relationship between the equation and the coefficients and measurements as follows:

$$\begin{aligned} &z(J+L)+z(J+L-1)c_{L-1}+\cdots+z(J+1)c_1 \\ &\quad+z(J)c_0=0 \quad J=-P,\cdots 0,\cdots,P-L \end{aligned} \tag{24}$$

For the convenience of the derivation, the $2P-L+1$ functions can be expressed in matrix form as follows:

$$\begin{bmatrix} z(-P) & z(-P+1) & \cdots & z(-P+L-1) \\ z(-P+1) & z(-P+2) & \cdots & z(-P+L) \\ \vdots & \vdots & \ddots & \vdots \\ z(P-L) & z(P-L+1) & \cdots & z(P-1) \end{bmatrix} \times \begin{bmatrix} c_0 \\ c_1 \\ \vdots \\ c_{L-1} \end{bmatrix} = -\begin{bmatrix} z(-P+L) \\ z(-P+L+1) \\ \vdots \\ z(P) \end{bmatrix} \tag{25}$$

This matrix clearly shows that the polynomial coefficient $[c_{L-1}, c_{L-2}, \cdots, c_0]$ can be obtained by the high-order cumulant vector $z$.

In practical applications, there can be only a limited number of snapshots. An estimation of the high-order cumulant matrices $\overline{C_1}$, $\overline{C_2}$ and $\overline{C_3}$ can be obtained using equation (26):

$$\begin{aligned} \overline{C_{4S}}=&\sum_{t=1}^{K}x_m(t)x_{-m}^*(t)x_p^*(t)x_{-p}(t) \\ &-\sum_{t=1}^{K}x_m(t)x_p^*(t)\sum_{t=1}^{K}x_{-m}^*(t)x_{-p}(t) \\ &-\sum_{t=1}^{K}x_m(t)x_{-m}^*(t)\sum_{t=1}^{K}x_p^*(t)x_{-p}(t) \\ &-\sum_{t=1}^{K}x_m(t)x_{-p}(t)\sum_{t=1}^{K}x_{-m}^*(t)x_p^*(t) \end{aligned} \tag{26}$$

Because the noise-free measurements $z$ are not available, their estimates $\bar{z}$ are used instead.

Substituting $\bar{z}$ into (25) instead of $z$ gives:

$$\overline{\boldsymbol{Z}}\overline{\boldsymbol{C}}=\overline{\boldsymbol{b}} \tag{27}$$

where

$$\overline{\boldsymbol{Z}}\widehat{=}\begin{bmatrix} \bar{z}(-P) & \bar{z}(-P+1) & \cdots & \bar{z}(-P+L-1) \\ \bar{z}(-P+1) & \bar{z}(-P+2) & \cdots & \bar{z}(-P+L) \\ \vdots & \vdots & \ddots & \vdots \\ \bar{z}(P-L) & \bar{z}(P-L+1) & \cdots & \bar{z}(P-1) \end{bmatrix},$$

$$\overline{\boldsymbol{C}}=\begin{bmatrix} \overline{c_0} \\ \overline{c_1} \\ \vdots \\ \overline{c}_{L-1} \end{bmatrix}, \quad \overline{\boldsymbol{b}}=-\begin{bmatrix} \bar{z}(-P+L) \\ \bar{z}(-P+L+1) \\ \vdots \\ \bar{z}(P) \end{bmatrix}$$

The polynomial coefficient $[c_{L-1}, c_{L-2}, \cdots, c_0]$ can then be estimated by minimizing the following penalty function:

$$\boldsymbol{G}(\boldsymbol{c})=\left\|\overline{\boldsymbol{Z}}\boldsymbol{c}-\overline{\boldsymbol{b}}\right\|_2^2 \tag{28}$$

Estimation of $[\overline{c_{L-1}}, \overline{c_{L-2}}, \cdots, \overline{c_0}]$ by minimizing $\boldsymbol{G}(\boldsymbol{c})$ is an open problem in the solution of these types of over-determined linear equation sets, with perturbations of a constrained structure on both sides. According to reference [21], the total least squares estimation provides only a small improvement over the ordinary least squares estimation and may destroy the structure of the data matrices. Moreover, reference [21] also shows that other solutions to linear equation sets with structured perturbations generally require too many computations. Therefore, we apply the ordinary least squares solution to estimate $\boldsymbol{c}$:

$$\overline{\boldsymbol{C}} = \overline{\boldsymbol{Z}}^{\dagger}\overline{\boldsymbol{b}} \tag{29}$$

where

$$\overline{\boldsymbol{Z}}^{\dagger} = (\overline{\boldsymbol{Z}}^{\boldsymbol{H}}\overline{\boldsymbol{Z}})^{-1}\overline{\boldsymbol{Z}}^{\boldsymbol{H}}.$$

Once the coefficient estimates are known, the DOA-dependent equation of (20) can be established as:

$$\overline{f(\chi)} = \chi^{L} + \overline{c_{L-1}}\chi^{L-1} + \cdots + \overline{c_1}\chi^{1} + \overline{c_0} = 0 \tag{30}$$

If the L roots are denoted by $\chi^k k = 1, 2, \cdots, L$, then the direction estimates are given by:

$$\theta_i = \sin^{-1}(\arg(\chi_k)\lambda/(4\pi d)) \quad i = 1, 2, \cdots, L \tag{31}$$

### B. RANGE ESTIMATION OF NEAR-FIELD SOURCES

Once the DOA estimation has been obtained, the next step is to obtain the range information of the near-field sources. The covariance matrix $\boldsymbol{R}$ is first constructed by the data received by sub-sensors 1 as follows:

$$\boldsymbol{R} = E[\boldsymbol{x}(t)\boldsymbol{x}^{H}(t)] = \boldsymbol{A}\boldsymbol{R}_s\boldsymbol{A}^{H} + \sigma^2 I \tag{32}$$

We implement the EVD of $\boldsymbol{R}$ as follows:

$$\boldsymbol{R} = \boldsymbol{U}\Lambda\boldsymbol{U}^{H} = \boldsymbol{U}_S\Lambda_S\boldsymbol{U}_S^{H} + \boldsymbol{U}_N\Lambda_N\boldsymbol{U}_N^{H} \tag{33}$$

where $\Lambda_S$ corresponds to the signal, and $\boldsymbol{U}_S$ spans the signal subspace of $\boldsymbol{R}$. $\Lambda_N$ corresponds to the noise, and $\boldsymbol{U}_N$ spans the noise subspace of $\boldsymbol{R}$.

Based on the conventional MUSIC algorithm, the angle information is substituted into $\boldsymbol{a}(\theta, r)$, and the minim of the following function are found:

$$r_i = \min(\boldsymbol{a}_{\theta_i,r}^{H}\boldsymbol{U}_N\boldsymbol{U}_N^{H}\boldsymbol{a}_{\theta_i,r}) \tag{34}$$

Traditional algorithms obtain the range information of the near-field sources by searching the spectrum, thus increasing the computation complexity. Additionally, the search step length limits the estimation precision. Therefore, the proposed algorithm utilizes the EVD method instead of spectrum searching to reduce the computational complexity.

To decrease the number of the dimensions requiring EVD, the following processing is performed:

$$\boldsymbol{a}_{\theta_i,r} = \boldsymbol{a}\boldsymbol{1}_{\theta_i}\boldsymbol{a}\boldsymbol{2}_r \tag{35}$$

$$\boldsymbol{a}\boldsymbol{1}_{\theta_i} = \Big[\mathrm{diag}(e^{j-(N)o_i}, e^{j(-(N)+1)o_i}\cdots 1\cdots e^{j((N)-1)o_i}, e^{j(N)o_i})\Big] \tag{36}$$

$$\boldsymbol{a}\boldsymbol{2}_r = [e^{j(N)^2\phi}\cdots 1\cdots e^{j(N)^2\phi}]^{T} \tag{37}$$

Substituting (35) into (34) yields:

$$r_i = \min(\boldsymbol{a}\boldsymbol{2}_r^{H}\boldsymbol{a}\boldsymbol{1}_{\theta_i}^{H}\boldsymbol{U}_N\boldsymbol{U}_N^{H}\boldsymbol{a}\boldsymbol{1}_{\theta_i}\boldsymbol{a}\boldsymbol{2}_r) \tag{38}$$

Equation (38) implies that $\boldsymbol{a}\boldsymbol{2}_r$ is the eigenvector corresponding to the smallest eigenvalue of the Hermitian matrix $\boldsymbol{a}\boldsymbol{1}_{\theta_i}^{H}\boldsymbol{U}_N\boldsymbol{U}_N^{H}\boldsymbol{a}\boldsymbol{1}_{\theta_i}$. Based on the eigenvector $\boldsymbol{a}\boldsymbol{2}_r$ obtained from the EVD of $\boldsymbol{a}\boldsymbol{1}_{\theta_i}^{H}\boldsymbol{U}_N\boldsymbol{U}_N^{H}\boldsymbol{a}\boldsymbol{1}_{\theta_i}$, $\boldsymbol{a}\boldsymbol{2}_r$ can be utilized to obtain the range information of the near-field sources.

$$\boldsymbol{a}\boldsymbol{2}_r(h)/\boldsymbol{a}\boldsymbol{2}_r(h+1) = e^{j((2h-1)\frac{\pi d^2\cos^2(\theta_i)}{\lambda r_i})} h \in [1, N] \tag{39}$$

$$r_i = \frac{\pi^2 d^2\cos(\theta_i)^2}{\lambda(\frac{1}{N}\sum_{h=1}^{N}(\frac{1}{2h-1}angle(\boldsymbol{a}\boldsymbol{2}_r(h)/\boldsymbol{a}\boldsymbol{2}_r(h+1))))}. \tag{40}$$

The proposed algorithm can avoid two-dimensional parameter matching and can also be applied to the problem of mixed sources estimation.

A description of the proposed algorithm is given as follows:

1. Construct the high-order cumulant vectors $z1$, $z2$ and $z3$. Combine these vectors to obtain the vector $z$:
2. Use equation (28) to obtain the polynomial coefficient $[\overline{c_{L-1}}, \overline{c_{L-2}}, \cdots, \overline{c_0}]$;
3. Substitute the polynomial coefficient $[c_{L-1}, c_{L-2}, \cdots, c_0]$ into the polynomial $f(\chi)$ and obtain the roots of the polynomial to obtain the angle information of the near-field source;
4. Construct the covariance matrix $\boldsymbol{R}$, and then implement the EVD of $\boldsymbol{R}$ to obtain the signal subspace $\boldsymbol{U}_S$ and the noise subspace $\boldsymbol{U}_N$;
5. Implement the EVD of $\boldsymbol{a}\boldsymbol{1}_{\theta_i}^{H}\boldsymbol{U}_N\boldsymbol{U}_N^{H}\boldsymbol{a}\boldsymbol{1}_{\theta_i}$ to obtain the eigenvector $\boldsymbol{a}\boldsymbol{2}_r$ corresponding to the smallest eigenvalue;
6. Estimate the range information of the near-field sources from (40).

## IV. IMPROVING THE PERFORMANCE OF THE PROPOSED ALGORITHM

The precision difference between the high-order cumulant vectors $z$ can be resolved intuitively by attaching a distinct weight to each vector in the penalty function (29). The slight difference between adjacent values of $z$ is negligible because of the large size of M; thus, another weighted penalty function can be defined according to (29) as follows:

$$\boldsymbol{W} = \mathrm{diag}(\boldsymbol{w}^{T}) = \mathrm{diag}([w_1, w_2, \cdots, w_{2P-L}]^{T}) \tag{41}$$

where

$$0 \le w_1, w_2, \cdots, w_{2P-L} \le 1,$$

and

$$w_1 + w_2 + \cdots + w_{2P-L} = 1.$$

Substituting the penalty function into function (29):

$$\begin{cases} w_1(z(-P+L)+z(-P+L-1)c_{L-1}+\cdots \\ +z(-P+1)c_1+z(-P)c_0)=0 \\ w_2(z(-P+L+1)+z(-P+L)c_{L-1}+\cdots \\ +z(-P+2)c_1+z(-P+1)c_0)=0 \\ \vdots \\ w_{2P-L}(z(P)+z(P-1)c_{L-1}+\cdots \\ +z(P-L+1)c_1+z(P-L)c_0)=0 \end{cases} \tag{42}$$

Function (42) can be expressed as follows:

$$\begin{aligned} &\mathrm{diag}(w_1, w_2, \cdots, w_{2P-L}) \\ &\times \begin{bmatrix} z(-P) & z(-P+1) & \cdots & z(-P+L-1) \\ z(-P+1) & z(-P+2) & \cdots & z(-P+L) \\ \vdots & \vdots & \ddots & \vdots \\ z(P-L) & z(P-L+1) & \cdots & z(P-1) \end{bmatrix} \\ &\times \begin{bmatrix} c_0 \\ c_1 \\ \vdots \\ c_{L-1} \end{bmatrix} = - \begin{bmatrix} w_1 z(-P+L) \\ w_2 z(-P+L+1) \\ \vdots \\ w_{2P-L} z(P) \end{bmatrix}. \end{aligned} \tag{43}$$

Because the value of the weighted coefficient $\boldsymbol{W}$ is associated with the precision of the high-order cumulant vector $z$, the higher the precision of $z$ is, the larger the weighted coefficient $\omega_i$ will be.

First, we will introduce the number of the elements used to construct the high-order cumulant vector $z$. There is only one element used to construct the high-order cumulant vectors $z2$ and $z3$. However, several elements are used to construct the high-order cumulant vector $z1$. The specific distribution is given in Figure 2.

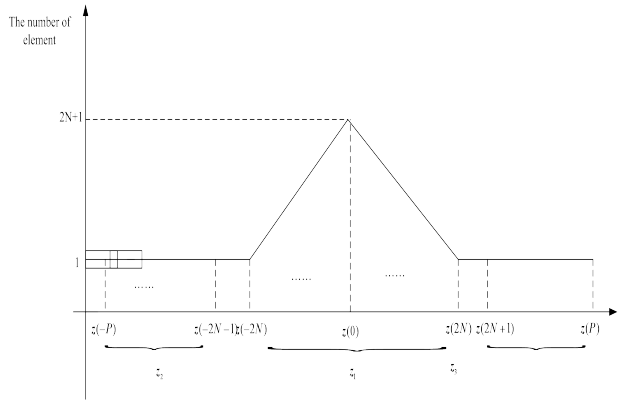


**FIGURE 2. Number of elements used to construct the high-order cumulant vector $z$.**

The high-order cumulant vector $z$ consists of three different types of vectors: $z1, z2$ and $z3$. Each element is composed differently and will have a higher precision where there arewith more elements. This principle is used to distribute the weight coefficients; the number of elements used in each equation is proportional to the weight coefficient. For example, the number of the elements that construct the high-order cumulant element is H; therefore, the weighted coefficient $w_i$ is also H. The specific distribution is given as follows:

$$\begin{cases} w_i = L1 \le i \le M(2N+1)-L+1 \\ w_i = (2N+1)M - i + \dfrac{1+L+i-(2N+1)M}{2} \\ \times (L+i-(2N+1)M) \\ M(2N+1)-L+1 < i \le (2N+1)M \\ w_i = (i-(2N+1)M)L + \dfrac{1+L}{2}L \\ (2N+1)M < i \le P-L+1 \\ w_i = d\dfrac{4N+2-L}{2}L + L - 1 \\ P-L+1 < i \le P \\ w_i = \dfrac{4N+2-L}{2}L - L(2N+1-i+P) \\ P < i \le P+2N-L \\ w_i = \dfrac{1+(P+2N-i)}{2}(P+2N-i) \\ +(L-P-2N+i) \\ P+2N-L < i \le P+2N \\ w_i = LP+2N \le i \le 2P+1-L. \end{cases} \tag{44}$$

Because the weighted coefficient $\boldsymbol{W}$ must meet the condition $w_1 + w_2 + \cdots + w_{2P-L} = 1$, it requires normalization to obtain the normalized weighted coefficient $\widehat{\boldsymbol{W}}_{SLS}$:

$$\widehat{\boldsymbol{W}}_{SLS} = \frac{\boldsymbol{W}}{\mathrm{sum}(\omega_i, i = 1, 2 \cdots 2P-L)}. \tag{45}$$

The weighted least squares (WLS) estimation of the equation coefficients can be obtained by substituting the weighted coefficient $\widehat{\boldsymbol{W}}_{SLS}$ into (29) and solving the least squares problem:

$$\overline{\boldsymbol{C}} = (\boldsymbol{W}_{SLS}\overline{\boldsymbol{Z}})^{\dagger}(\boldsymbol{W}_{SLS}\overline{\boldsymbol{b}}). \tag{46}$$

The signal DOA can then be estimated following the steps given in Section 3.

## V. PERFORMANCE ANALYSIS OF THE PROPOSED ALGORITHM

### A. ANALYSIS OF THE MAXIMUM NUMBER OF ESTIMATED SOURCES

The values of the maximum number of sources estimated by the proposed algorithm, the two-stage MUSIC (TSMUSIC) algorithm and the mixed-order MUSIC (MOMUSIC) algorithm are considered. Assuming that there are Q sensors, which include 2N+1 sensors in sub-sensor1, M arrays in sub-sensor 2 and M arrays in sub-sensor 3, the proposed algorithm can localize (2N+1)+(2N+1)M sources, the TSMUSIC algorithm can localize Q-1 sources, and the MOMUSIC algorithm can localize M+N+MN sources. The analysis above shows that the proposed algorithm can estimate a much larger number of sources than the other two algorithms. If the number of arrays is fixed, then the array aperture of the

TSMUSIC algorithm will not change, whereas the number of sub-sensors will change the number of sources estimated by the proposed algorithm and the TSMUSIC algorithm. A certain combination exists that will maximize the number of sources estimated by the proposed algorithm and the TSMUSIC algorithm.

### B. ANALYSIS OF THE COMPUTATIONAL COMPLEXITY

In contrast with far-field source estimation, near-field sources must estimate two parameters: angle information and range information. Therefore, we analyze the computational complexity from two aspects. The number of the angle space spectra is assumed to be $J_1$, and the number of the range space spectra is assumed to be $J_2$. The computational complexity of the proposed algorithm, the TSMUSIC algorithm and the MOMUSIC algorithm are analyzed for the same number of the sensors.

To analyze the computational complexity, the main contributors are considered to be the multiplications involved in the cumulant matrix construction, the EVD implementation, and the MUSIC spectral search.

The computational complexity of the TSMUSIC algorithm is therefore:

$$\begin{aligned} &C_{TSMUSIC} \\ &= C_{D-TSMUSIC} + C_{R-TSMUSIC} \\ &= (4(M+N)+1)^2(15K) + 2(4(M+N)+1)^2(L+2) \\ &\quad + (2(M+N)+1)^2(15K) + (2(M+N)+1)^2(L+2) \\ &\quad + J_1(2(M+N)+1-L)(2(M+N)+2). \end{aligned}$$

The computational complexity of the MOMUSIC algorithm is:

$$\begin{aligned} &C_{MOMUSIC} \\ &= C_{R-MOMUSIC} + C_{D-MOMUSIC} \\ &= (2(M+N)+1)^2(L+2) \\ &\quad + J_2(2(M+N)+1-L)(2(M+N)+2) \\ &\quad + (2(M+1)(N+1)+1)(15K) \\ &\quad + ((M+1)(N+1)+1)^2(L+2) \\ &\quad + J_1((M+1)(N+1)+1-L)((M+1)(N+1)+1+2). \end{aligned}$$

The computational complexity of the proposed algorithm is:

$$\begin{aligned} C &= C_D + C_R \\ &= (2M(2N+1)+N^2)(15K) + 2(2N+1)^2(L+2). \end{aligned}$$

To demonstrate the computational complexity of the three algorithms, we use the same values for the three algorithms: the number of arrays is 23 ($M = 3$, $N = 8$), the number of snapshots is $K = 100$, the angle search step is 0.5° ($J_1 = 360$), and the range search step is $0.1\lambda$ ($J_2 = 150$). The computational complexity of the proposed algorithm, the TSMUSIC algorithm and the MOMUSIC algorithm are shown in Table 1 (A, B and C represent the computation time for the proposed algorithm, the TSMUSIC algorithm and the MOMUSIC algorithm, respectively).

**TABLE 1. Comparison of the complexity of various algorithms.**

| $N=8, M=3, K=100, J_1=360, J_{rough2}=150$ | |
|---|---|
| A | 250734 |
| B | 4034817 |
| C | 658479 |
| B / A | 16.09 |
| C / A | 2.626 |

It can be seen that the computational complexity of the proposed algorithm is much lower than that of the other two algorithms, in agreement with the analysis above from Table 1.

## VI. SIMULATION

This section describes some simulations that are conducted to assess the proposed algorithm. We consider a 23-element (M = 3, N = 8) sensor with element spacing of $d_{\min} = \lambda/4$. In all, 200 Monte-Carlo runs are performed to obtain the experimental results; the root mean square error (RMSE) of the results is expressed as:

$$RMSE = \sqrt{\sum_{k=1}^{L}\sum_{n=1}^{M}(\hat{\alpha}_k - \alpha_k)^2/ML}$$

where $\hat{\alpha}_k$ and $\alpha_k$ represent the estimation value and the true value, respectively, of the DOA $\theta_k$ or the range $r_k$.

In the first experiment, we consider two signals. The two near-field sources are located at (30°, 4λ) and (35°, 2λ). The experiment is based on the same conditions as above.

1) RMSE versus SNR: the number of snapshots is fixed at 300, while the SNR varies from 0 to 30 dB. The RMSE of the azimuth DOA and the range estimations are shown in Figure 3 and Figure 4, respectively. It can be seen that the proposed algorithm outperforms the methods described in references [7] and [9] in estimation accuracy of the azimuth DOA and the range for all values of the SNR. The novel array model adopted by the proposed algorithm can thus greatly extend the array aperture. Additionally, the proposed algorithm combines CEM methods to improve the precision of the parameter estimation. Because a spectral search is not required, the performance of the proposed algorithm will not be affected by the value of the spectrum search step.

2) RMSE versus the number of snapshots: the SNR is fixed at 10 dB, while the number of snapshots varies from 100 to 500. The RMSE values of the azimuth DOA and range

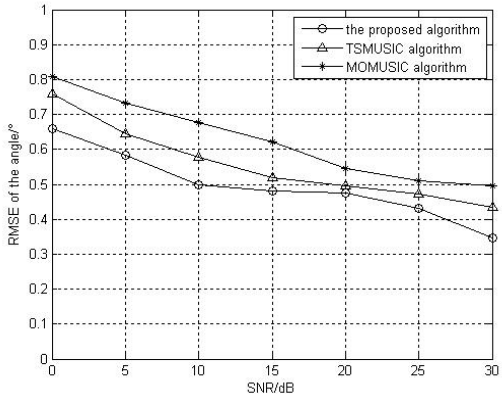


**FIGURE 3.** Relationship between the RMSE of the angle and the SNR.

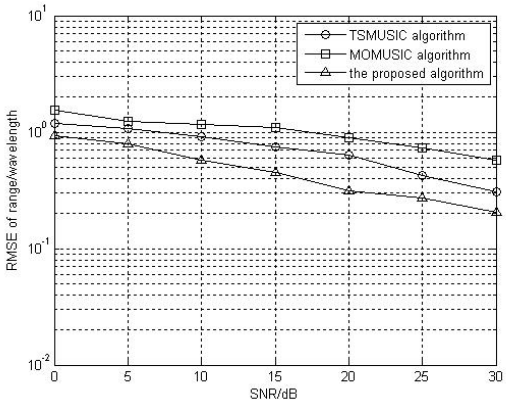


**FIGURE 4.** Relationship between the RMSE of the range and the SNR.

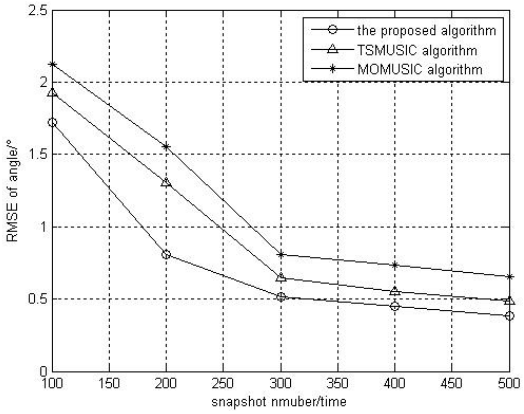


**FIGURE 5.** Relationship between the RMSE of the angle and the snapshots.

estimations are shown in Figure 5 and Figure 6, respectively. It can be seen that the proposed algorithm outperforms the methods described in references [10] and [12] in terms of the estimation accuracy of the azimuth DOA and the range for all values of the number of snapshots. The proposed algorithm adopts the novel array model that can extend the array aperture greatly. Moreover, combining the proposed algorithm with CEM methods can improve the precision of

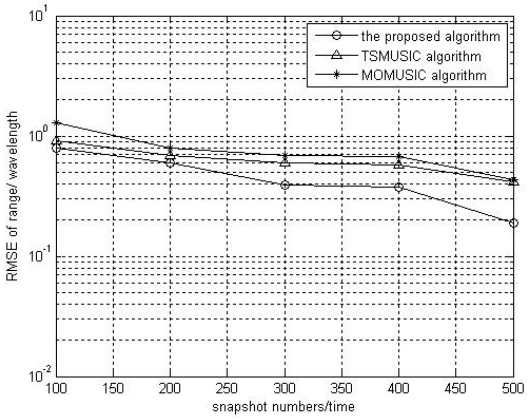


**FIGURE 6.** Relationship between the RMSE of the range and the snapshots.

the parameter estimation. The proposed algorithm does not require the spectrum search; therefore, the performance of the proposed algorithm would not be affected by the step of the spectrum search.

In the second experiment, two signals are considered. The two near-field sources are located at $(30°, 4\lambda)$ and $(35°, 2\lambda)$. The number of snapshots is fixed at 300, the SNR is fixed at 20 dB and the number of arrays is varied from 11 to 21. The statistical simulation times are shown in Table 2 (A, B and C represent the computation times of the proposed algorithm, the TSMUSIC algorithm and the MOMUSIC algorithm, respectively).

**TABLE 2.** Computation times for different numbers of sensors.

| | | | | | |
|---|---|---|---|---|---|
| A/s | 0.3396 | 0.443847 | 0.563218 | 0.689559 | 0.835418 |
| B/s | 3.0142 | 4.1215 | 5.0112 | 7.032 | 7.564 |
| C/s | 1.0188 | 1.3314 | 1.6895 | 1.8618 | 2.350625 |

It is clear that the proposed algorithm has a much lower running time than the other two algorithms. Because the TSMUSIC algorithm and the MOMUSIC algorithm both require eigenvalue decomposition and spectrum search, they are influenced by the number of arrays. Both algorithms will have a longer running time if there are more arrays. However, the proposed algorithm does not require eigenvalue decomposition and a spectrum search, and thus the running time is not influenced by the number of arrays. The increase in performance of the proposed algorithm is more evident as the number of arrays is increased.

For the third experiment, twelve signals are considered. The twelve near-field sources are located at $(60°, 5\lambda)$, $(50°, 6\lambda)$, $(40°, 4\lambda)$, $(30°, 5\lambda)$, $(20°, 5\lambda)$, $(10°, 6\lambda)$, $(-60°, 6\lambda)$, $(-50°, 4\lambda)$, $(-40°, 5\lambda)$, $(-30°, 3\lambda)$, $(-20°, 5\lambda)$ and $(-10°, 3\lambda)$. The number of arrays is 13 ($N = 4, M = 2$), the SNR is fixed at 20dB and the number of snapshots is fixed at 300. The proposed algorithm adopts the spectrum

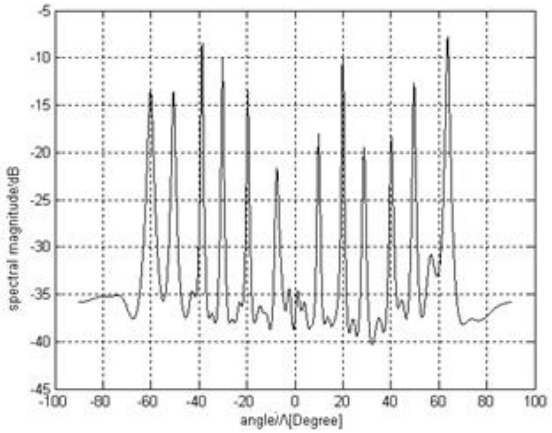


**FIGURE 7.** Spatial spectrum of the proposed algorithm.

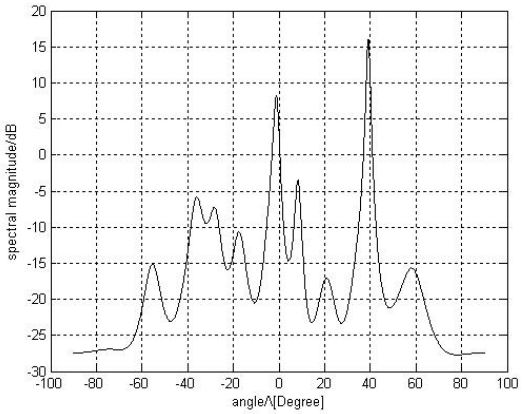


**FIGURE 8.** Spatial spectrum of the TSMUSIC algorithm.

search instead of getting the roots of the polynomial in order to demonstrate the performance of the array aperture extension of the proposed algorithm. The spectrum of the proposed algorithm is shown in Figure 7. The spectrum of the TSMUSIC algorithm is shown in Figure 8.

The proposed algorithm can estimate the twelve signals successfully, while the TSMUSIC algorithm is unsuccessful. This is because the proposed algorithm adopts a special novel sensor model and combines the high-order cumulant vector. Compared with the TSMUSIC algorithm, the proposed algorithm has the ability to extend the sensor aperture. The simulation results are consistent with the analysis above.

In the fourth experiment, some simulations are conducted to assess the proposed algorithm and the improved algorithm. Since the improved algorithm only optimizes the angle estimation, only the RMSE of the angle estimation is considered in this simulation. This experiment has the same conditions as the experiments above.

RMSE versus SNR: The two near-field sources are located at $(30°, 4\lambda)$ and $(35°, 2\lambda)$. The number of snapshots is fixed at 300, and the SNR is varied from 0 to 30dB. The RMSE of the azimuth DOA estimation is shown in Figure 9. It can be seen that the improved algorithm outperforms the proposed

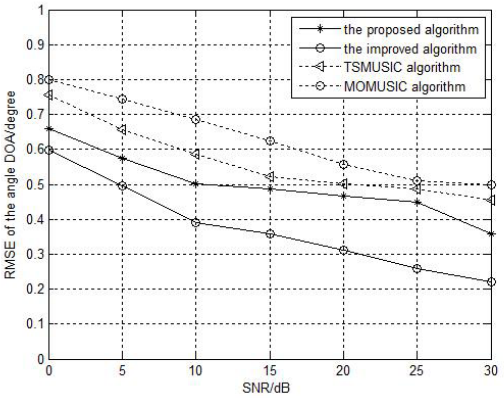


**FIGURE 9.** Relationship between RMSE of the angle and SNR.

algorithm in terms of the estimation accuracy of the azimuth DOA for all values of the SNR. The improved algorithm adopts to weighted coefficient matrix that can improve the accuracy of the vehicle positioning.

## VII. CONCLUSION

In this paper, a novel sensor model was presented to locate a vehicle. The proposed algorithm introduces a new sensor model combined with a high-order cumulant matrix to extend the array aperture. Additionally, the proposed algorithm adopts the CEM method, which can decrease the computational complexity. To improve the accuracy of the vehicle positioning, the algorithm was improved by introduction of a weighted coefficient matrix. The simulation results showed that the proposed algorithm has a lower computational complexity and a higher utilization of sensors; in addition, the proposed algorithm also avoids two-dimensional parameter matching, and the improved algorithm has a higher precision for the vehicle positioning.

## REFERENCES

[1] L. Wan, G. Han, L. Shu, S. Chan, and N. Feng, "PD source diagnosis and localization in industrial high-voltage insulation system via multimodal joint sparse representation," *IEEE Trans. Ind. Electron.*, vol. 63, no. 4, pp. 2506–2516, Apr. 2016.

[2] R. Schmidt, "Multiple emitter location and signal parameter estimation," *IEEE Trans. Antennas Propag.*, vol. AP-34, no. 3, pp. 276–280, Mar. 1986.

[3] L. Wan, G. Han, L. Shu, S. Chan, and T. Zhu, "The application of DOA estimation approach in patient tracking systems with high patient density," *IEEE Trans. Ind. Informat.*, vol. 12, no. 6, pp. 2353–2364, Dec. 2016.

[4] X. Zhang and D. Xu, "Low-complexity ESPRIT-based DOA estimation for colocated MIMO radar using reduced-dimension transformation," *Electron. Lett.*, vol. 47, no. 4, pp. 283–284, Feb. 2011.

[5] L. Wan, G. Han, L. Shu, and N. Feng, "The critical patients localization algorithm using sparse representation for mixed signals in emergency healthcare system," *IEEE Syst. J.*, vol. 12, no. 1, pp. 52–63, Mar. 2018.

[6] A. L. Swindlehurst and T. Kailath, "Passive direction-of-arrival and range estimation for near-field sources," in *Proc. 4th Annu. ASSP Workshop Spectr. Estimation Modeling*, Minneapolis, MN, USA, Aug. 1988, pp. 123–128.

[7] Y.-D. Huang and M. Barkat, "Near-field multiple source localization by passive sensor array," *IEEE Trans. Antennas Propag.*, vol. 39, no. 7, pp. 968–975, Jul. 1991.

[8] W. Zhi and M. Y. W. Chia, "Near-field source localization via symmetric subarrays," *IEEE Signal Process. Lett.*, vol. 14, no. 6, pp. 409–412, Jun. 2007.

[9] Y. Zhou, D. Z. Feng, and J. Q. Liu, "A new subspace method for estimation of parameters of near field sources," *J. Xian Univ.*, vol. 33, no. 1, pp. 41–45, Feb. 2006.

[10] J. Liang and D. Liu, "Passive localization of mixed near-field and far-field sources using two-stage MUSIC algorithm," *IEEE Trans. Signal Process.*, vol. 58, no. 1, pp. 108–120, Jan. 2010.

[11] G. Liu and X. Sun, "Two-stage matrix differencing algorithm for mixed far-field and near-field sources classification and localization," *IEEE Sensors J.*, vol. 14, no. 6, pp. 1957–1965, Jun. 2014.

[12] B. Wang, J. Liu, and X. Sun, "Mixed sources localization based on sparse signal reconstruction," *IEEE Signal Process. Lett.*, vol. 19, no. 8, pp. 487–490, Aug. 2012.

[13] J. J. Jiang, F. J. Duan, J. A. Chen, Y.-C. Li, and X.-N. Hua, "High-accuracy localization algorithm for mixed near-and far-field sources," *J. Tianjin Univ. Sci. Technol.*, vol. 46, no. 12, pp. 1114–1120, Dec. 2013.

[14] R. Jeffers, K. L. Bell, and H. L. Van Trees, "Broadband passive range estimation using MUSIC," in *Proc ICASSP*, Orlando, FL, USA, Apr. 2002, pp. 2920–2923.

[15] J. C. Chen, R. E. Hudson, and K. Yao, "Maximum-likelihood source localization and unknown sensor location estimation for wideband signals in the near-field," *IEEE Trans. Signal Process.*, vol. 50, no. 8, pp. 1843–1854, Aug. 2002.

[16] D. Starer and A. Nehorai, "Passive localization of near-field sources by path following," *IEEE Trans. Signal Process.*, vol. 42, no. 3, pp. 677–680, Mar. 1994.

[17] A. J. Weiss and B. Friedlander, "Range and bearing estimation using polynomial rooting," *IEEE J. Ocean. Eng.*, vol. 18, no. 2, pp. 130–137, Apr. 1993.

[18] R. N. Challa and S. Shamsunder, "High-order subspace-based algorithms for passive localization of near-field sources," in *Proc. 29th Asilomar Conf Signals, Syst. Comput.*, Pacific Grove, CA, USA, Oct./Nov. 1995, pp. 777–781.

[19] N. Yuen and B. Friedlander, "Performance analysis of higher order ESPRIT for localization of near-field sources," *IEEE Trans. Signal Process.*, vol. 46, no. 3, pp. 709–719, Mar. 1998.

[20] Y. T. Wu, Y. B. Zhang, and H. Cao, "The fast algorithm for the four dimensional parameter estimation of a single near-field source based on the uniform circular array," *J. Wuhan Inst. Technol.*, vol. 35, no. 3, pp. 75–78, Mar. 2013.

[21] P. Pal and P. P. Vaidyanathan, "Nested arrays: A novel approach to array processing with enhanced degrees of freedom," *IEEE Trans. Signal Process.*, vol. 58, no. 8, pp. 4167–4181, Apr. 2010.

[22] K. Han and A. Nehorai, "Nested array processing for distributed sources," *IEEE Signal Process. Lett.*, vol. 21, no. 9, pp. 1111–1114, Sep. 2014.

[23] Z.-M. Liu, Z.-T. Huang, and Y.-Y. Zhou, "Computationally efficient direction finding using uniform linear arrays," *IET Radar, Sonar Navigat.*, vol. 6, no. 1, pp. 39–48, Jan. 2012.

[24] H. Jin, M. N. S. Swamy, and M. O. Ahmad, "Efficient application of MUSIC algorithm under the coexistence of far-field and near-field sources," *IEEE Trans. Signal Process.*, vol. 60, no. 4, pp. 2066–2070, Apr. 2012.

[25] R. Deng, Z. Yang, M.-Y. Chow, and J. Chen, "A survey on demand response in smart grids: Mathematical models and approaches," *IEEE Trans. Ind. Informat.*, vol. 11, no. 3, pp. 570–583, Jun. 2015.

[26] R. Deng, J. Chen, X. Cao, Y. Zhang, S. Maharjan, and S. Gjessing, "Sensing-performance tradeoff in cognitive radio enabled smart grid," *IEEE Trans. Smart Grid*, vol. 4, no. 1, pp. 302–310, Mar. 2013.


**XIAOLIN LI** received the Ph.D. degree from the School of Information and Communication Engineering, Harbin Engineering University, in 2016. She is currently a Lecturer at Yantai University. Her research interests are mostly focused on array signal processing, space spectrum estimation, anti-radar decoy, and so on.

**SHIE WU** received the Ph.D. degree from the School of Information and Communication Engineering, Beijing University of Posts and Telecommunications, in 2016. She is currently a Lecturer at Yantai University. Her research interests are mostly focused on wireless and mobile communication theory and technology, 5G dense small cell network energy efficiency optimization, interference management, base station collaboration, and resource management.

**JIQU HAN** received the degree in electronic engineering from the Harbin Institute of Marine Engineering in 1989, and the master's degree in naval aeronautical engineering from the Institute of Communication and Information System in 2005. He is currently an Associate Professor with Yantai University. His research interests are mostly focused on signal and information processing, and remote sensing image processing.

**WENQI WANG** is currently pursuing the master's degree with Yantai University. Her research interests include mobile image processing and lane detection.